Molecular Physics, Vol. 103, No. 19, 10 October 2005, 2675–2685

Taylor & Francis
Taylor & Francis Group

The compression of polymer brushes under shear: the friction coefficient as a function of compression, shear rate and the properties of the solvent

F. GOUJON†, P. MALFREYT*† and D. J. TILDESLEY‡

†Laboratoire de Thermodynamique des Solutions et des Polymères, UMR CNRS 6003, Université Blaise Pascal, 24 avenue des Landais, 63177 Aubière Cedex, France

‡Unilever Research Port Sunlight, Bebington, Wirral, UK CH63 3JW

(*Received 3 March 2005; accepted 14 April 2005*)

We present a study of the compression of polymer-grafted surfaces using the dissipative particle dynamics (DPD) method at constant chemical potential. We demonstrate the importance of performing simulations of compression at fixed chemical potential of the solvent by comparing the simulated force-compression curves at constant chemical potential and density with the experimental profile determined for poly(ethylene-propylene) chains grafted onto mica surfaces in a cyclohexane solvent. The simulated force-distance and friction profiles are presented as a function of the polymer grafting density, the shear rate and the nature of the solvent. We also study the influence of the steepness of conservative potential between polymer segments and the size of the solvent elements (particles) on the form of the force-compression and friction-compression profiles.

1. Introduction

The effective friction coefficient between two smooth solid surface immersed in toluene when they are in lateral motion under a given normal load is about 0.6. Covering these surfaces with polystyrene dramatically reduces the friction by as much as two orders of magnitude [1]. This type of surface layer formed when polymers are grafted by a chain end to a surface at a high coverage is called a polymer brush. It is used in a variety of applications including the protection of surfaces and their lubrication.

Over the past ten years, the surface force apparatus (SFA) has been used extensively to measure both static and dynamic forces between smooth and grafted polymer surfaces. The SFA was initially used to determine normal forces between polymer brushes at equilibrium [2–4]. The technique has been extended to measure simultaneously the normal and shear forces between two polymer bearing surfaces in relative lateral motion [5–9]. A large number of normal and shear force profiles have been determined experimentally as a function of the surface separation and these results have been interpreted using both theory [10–14] and simulation [15–18].

A molecular understanding of the friction between compressed polymer brushes is difficult to access experimentally [9, 16, 19, 20] and a suitable simulation method has to explore the length and time scales for polymer relaxation in the presence of a solvent. This points us towards a coarse-grained model of the system and a mesoscopic simulation method. We have already established that dissipative particle dynamics (DPD) can reproduce the equilibrium [21] and rheological [22] properties of polymer brushes. In a recent paper [23], we have calculated the force-distance profiles of compressed polymer brushes using DPD in the grand canonical ensemble, where the solvent between the two surfaces is in equilibrium with a reservoir of the bulk fluid at the same temperature and chemical potential. We have shown that under conditions of constant chemical potential the shape of the force-distance profile agrees well with experiment and with the SCF theory if the appropriate assumptions are made about the shape of the polymer density profile.

In this paper, we extend the DPD simulations of equilibrium polymer brushes in the grand canonical ensemble to study compressed polymer brushes under shear. We are concerned with understanding how the polymer and solvent properties can influence

*Corresponding author.
Email: patrice.malfreyt@univ-bpclermont.fr

Molecular Physics
ISSN 0026–8976 print/ISSN 1362–3028 online
http://www.tandf.co.uk/journals
DOI: 10.1080/00268970500134706

the friction as a step towards a molecular understanding of friction. In particular, we address the following questions:

(1) How does the friction coefficient change under compression at constant chemical potential of the solvent?
(2) Does the presence of the solvent affect the friction coefficient?
(3) How do the grafting density and the shear rate change the frictional forces?
(4) How does the steepness of the conservative potential between polymer segments and the size of solvent particle affect the friction?

The paper is organized as follows. In section 2, we describe the DPD model. In section 3, we outline the polymer brush system and we present the thermodynamic, rheological and structural properties calculated in this work. We demonstrate the stability of the method at fixed chemical potential in section 4 and we discuss the influence of the shear rate and grafting density on the friction profiles for wet and dry brushes in section 5. Section 6 considers the influence of the form of conservative potential between polymer segments and the size of the solvent elements or particles on the friction coefficient. Section 7 contains our conclusions.

2. The DPD simulation method

DPD describes a system in term of N particles with mass m_i, whose positions $\mathbf{r}_i$ and velocities $\mathbf{v}_i$ move according to the Newton's equation of motion

$$\frac{\mathrm{d}\mathbf{r}_i}{\mathrm{d}t} = \mathbf{v}_i, \quad m_i \frac{\mathrm{d}\mathbf{v}_i}{\mathrm{d}t} = \mathbf{f}_i \tag{1}$$

where t represents time, $\mathbf{f}_i$ the total force acting on the ith particle. The total force $\mathbf{f}_i$ contains three pairwise additive contributions

$$\mathbf{f}_i = \sum_{j \neq i} \left(\mathbf{f}_{ij}^C + \mathbf{f}_{ij}^D + \mathbf{f}_{ij}^R \right). \tag{2}$$

The conservative repulsive force $\mathbf{f}_{ij}^C$ derives from a soft interaction potential and is expressed as follows

$$\mathbf{f}_{ij}^C = \begin{cases} a_{ij}\, \omega_C(r_{ij})\, \mathbf{e}_{ij} & (r_{ij} < r_c) \\ 0 & (r_{ij} \geq r_c) \end{cases} \tag{3}$$

where a_{ij} is the maximum repulsion between particles i and j, r_c is the cutoff radius and $\mathbf{r}_{ij} = \mathbf{r}_i - \mathbf{r}_j$, $r_{ij} = |\mathbf{r}_{ij}|$ and $\mathbf{e}_{ij} = \mathbf{r}_{ij}/r_{ij}$. The weight function $\omega_c(r_{ij})$ vanishes for $r_{ij} > r_c$. The dissipative $\mathbf{f}_{ij}^D$ and random forces $\mathbf{f}_{ij}^R$ are given by

$$\mathbf{f}_{ij}^D = -\gamma\, \omega_D(r_{ij}) (\mathbf{e}_{ij} \cdot \mathbf{v}_{ij}) \mathbf{e}_{ij} \tag{4}$$

$$\mathbf{f}_{ij}^R = \sigma\, \omega_R(r_{ij})\, \zeta_{ij}\, \mathbf{e}_{ij}\, (\delta t)^{-1/2} \tag{5}$$

where δt is the time step, $\mathbf{v}_{ij} = \mathbf{v}_i - \mathbf{v}_j$. $\omega_D(r_{ij})$ and $\omega_R(r_{ij})$ are additional dimensionless weighting functions, also vanishing for $r_{ij} > r_c$. γ and σ are the dissipation strength and noise strength, respectively. ζ_{ij} is a independent random Gaussian variable with zero mean and unit variance for each pair (i, j) of particles. $\zeta_{ij} = \zeta_{ji}$ is required to satisfy the Newton's third law. The DPD method has been shown to produce a constant-NVT ensemble as the following relations are satisfied [24]

$$\omega_D(r_{ij}) = (\omega_R(r_{ij}))^2 \quad \text{and} \quad \sigma^2 = 2k_B T \gamma \tag{6}$$

where k_B is Boltzmann's constant, T is the temperature.

In our DPD model, the units are dimensionless. All the particles are equal mass, $m_i = m = 1$. The unit of length is r_c and the unit of energy is $k_B T$. All the simulations are carried out using $k_B T = 2.0$. The particles in DPD do not represent individual molecules or atoms but rather describe the position and momentum of a region of the fluid or a group of monomers in the case of the modelling of polymer chains. To be consistent with this coarse-graining description, any conservative force introduced would be soft and mainly repulsive. The weight functions $\omega_D(r_{ij})$ and $\omega_R(r_{ij})$ are chosen as in previous work [21–23, 25] and are of the form

$$\omega_D(r_{ij}) = (\omega_R(r_{ij}))^2 = \begin{cases} (1 - r_{ij}/r_c)^2 & (r_{ij} < r_c) \\ 0 & (r_{ij} \geq r_c) \end{cases} \tag{7}$$

For computational convenience, we keep the conservative force truncated at the cutoff radius r_c. Usually [21–23, 25], the weighting function $\omega_C(r_{ij})$ takes the form

$$\omega_C(r_{ij}) \begin{cases} (1 - r_{ij}/r_c) & (r_{ij} < r_c) \\ 0 & (r_{ij} \geq r_c). \end{cases} \tag{8}$$

Throughout this paper, we also use two other analytical expressions for this weighting function in order to study the influence of the conservative interaction on the friction coefficient. In all cases, the conservative force remains truncated at r_c. The decrease in the particle size will be accomplished by decreasing the cutoff radius r_c for all the weighting functions. The equations of motions are integrated using a modified version of the velocity-Verlet algorithm [25] using a timestep δt of 0.02 in reduced units.

The presence of the random and dissipative forces apparently makes the DPD similar to the Brownian dynamics (BD). However, we see that all the forces in DPD are pairwise additive, central and obey Newton's third law leading to a conservation of linear and angular momentum. Theses features are essential to recover hydrodynamics behaviour. In BD, the momentum is not longer conserved and the macroscopic behaviour will not be hydrodynamic. Additionally, in most applications of BD, the solvent is not simulated explicitly.

3. Simulation of the polymer brushes system

The model used to describe the polymer brush system is composed of polymer chains, solvent particles and two planar surfaces. The periodic boundary conditions are applied in the x and y directions; in the z direction the particles are confined by the two grafted surfaces. The polymer chains are grafted to the surfaces to form two polymer brushes, one on the top and the other on the bottom of the box, as shown in figure 1. Two different grafting densities σ_g (1/3 and 1/6) are used here. An additional conservative spring force is used to connect the neighbouring beads of the homopolymer chain. Each grafted linear chain contains 20 beads. The simulations are carried out in good solvent conditions by making both the a_{ij} parameter for the polymer-solvent interactions equal to 40 and the a_{ij} for the remaining interactions equal to 60. We define h as the distance between the grafting surfaces and h_0 as the distance between the surfaces at which the interpenetration between the two layers vanished. The system for which the distance between the grafted surfaces is h_0 is considered as the reference system and h/h_0 is called the compression.

Previously, we have established a methodology in the grand canonical ensemble for the study of the compression of equilibrium grafted polymer brushes [23] and we have checked the thermal, mechanical and chemical equilibrium of the DPD method in the constant-μVT ensemble. In this paper, we extend the methodology to the study of the compressed polymer brushes under shear. We take care to use sufficiently high values of σ and γ ($\sigma = 7.07$, $\gamma = 12.5$) in order to maintain a constant profile of temperature across the pore. The methodology for keeping the chemical potential of the solvent constant under shear remains the same as that used at equilibrium, except for choosing the velocity of the created solvent particle. In the case of no shear, when a creation is accepted, the velocity of the solvent particle is chosen from a Gaussian distribution with zero mean and $\sqrt{(k_B T)}$ variance. To take into account the shear along the x-direction, the x-component of the solvent particle's velocity is changed by the addition of the x-component of the streaming velocity. The shear is induced by moving the lattice points associated with particles of the surface in the top and bottom surface in opposite directions along the x-axis by a distance δx defined by

$$\delta x = \pm(1/2)\dot{\gamma}_a L_z \delta t \tag{9}$$

where $\dot{\gamma}_a$ is the steady uniform shear rate and L_z is the dimension of the cell along the z direction. Throughout this work, two typical values of $\dot{\gamma}_a$ are used: $\dot{\gamma}_a = 0.1$ and $\dot{\gamma}_a = 0.05$. Further details concerning both the structure of the system and the simulation can be found in a previous paper [23].

3.1. *Thermodynamic properties*

The components of the pressure tensor along the z-axis is calculated using the Irving-Kirkwood [26, 27] definition. The profiles of the pressure are calculated as a function of z by splitting the cell into slabs of width Δz. The $p_{\alpha\beta}$ component is composed of a

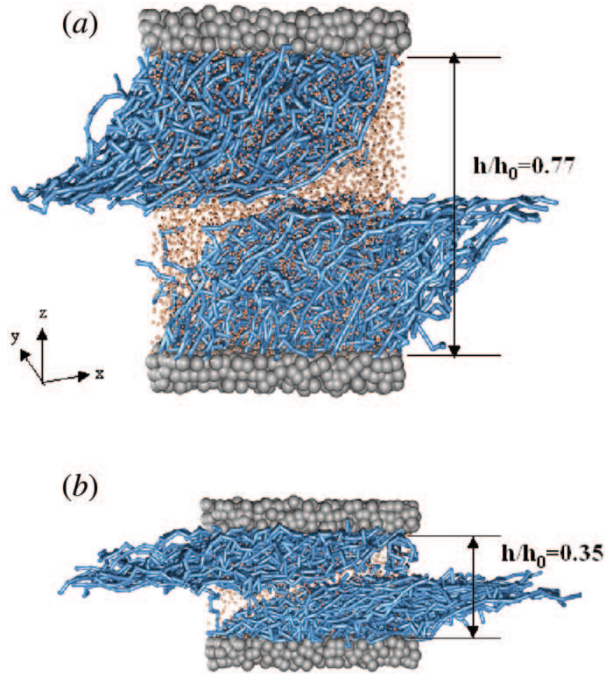

Figure 1. Typical configurations for the polymer brushes system in good solvent conditions under shear at two surface separations. (*a*) $h/h_0 = 0.77$ and (*b*) $h/h_0 = 0.35$. The polymer chains are represented using sticks and the open circles represent solvent particles. The grafted surfaces are represented by bigger grey open particles.

kinetic contribution $p_{\alpha\beta}^{\mathrm{kin}}(z)$ and of a virial part $p_{\alpha\beta}^{\mathrm{conf}}(z)$ defined as

$$p_{\alpha\beta}^{kin}(z) = \frac{1}{V}\left\langle \sum_{i,\alpha,\beta} H(z_i) m_i \left[(v_i)_\alpha - (u)_\alpha\right]\left[(v_i)_\beta - (u)_\beta\right]\right\rangle \tag{10}$$

where $\langle\cdots\rangle$ denotes the configurational average and α and β represent x, y and z directions, m_i and $(v_i)_\alpha$ are the mass and velocity of particle i, respectively. $V = L_x L_y \Delta z$ is thus the volume of the basic slab, $H(z_i)$ is a top-hat function and $(u)_\alpha$ is the α component of the streaming velocity. Whereas $(u)_x$ is a measure of the induced flow field, $(u)_y$ and $(u)_z$ are essentially zero for all z.

$$p_{\alpha\beta}^{\mathrm{conf}}(z) = \frac{1}{A}\left\langle \sum_{i=1}^{N-1}\sum_{j>i}^{N} (r_{ij})_\alpha (\mathrm{f_{ij}})_\beta \frac{1}{|z_{\mathrm{ij}}|}\theta\left(\frac{z - z_{\mathrm{i}}}{z_{\mathrm{ij}}}\right)\theta\left(\frac{z_{\mathrm{j}} - z}{z_{\mathrm{ij}}}\right)\right\rangle \tag{11}$$

where f_{ij} represents the sum of the conservative, random and dissipative contributions and θ is a unit step function.

For a system with an inhomogeneity in density in the z direction, the configurational chemical potential $\mu^{\mathrm{conf}}(z)$ [28–30] depends on the z position, so

$$\mu^{\mathrm{conf}}(z) = k_B T \ln\left[\frac{\langle\rho(z)\rangle}{\langle\exp(-\Delta U^{\mathrm{test}}/k_B T)\rangle}\right] \tag{12}$$

where $\rho(z)$ is the number density and ΔU^{test} is the interaction energy of the test particle, at height z, with the other N particles in the box.

3.2. *Rheological properties*

The appropriate rheological properties of the system are the friction coefficient and the viscosity. The profiles of the friction coefficient ϵ and viscosity η are calculated along the z-axis as

$$\epsilon(z) = -\frac{\langle p_{xz}(z)\rangle}{\langle p_{zz}(z)\rangle} \tag{13}$$

$$\eta(z) = -\frac{\langle p_{xz}(z)\rangle}{\langle \mathrm{d}u_x(z)/\mathrm{d}z\rangle}. \tag{14}$$

Previous [22] study showed from the viscosity profiles that the minimum of the viscosity was observed in the middle of the pore in the region of the highest solvent density. The value of viscosity used in this paper represents the viscosity in the middle of the pore.

3.3. *Structural properties*

The mean square radius of gyration is usually used to define the characteristic size of a polymer chain and is defined as

$$R_g^2 = \frac{1}{N_b}\sum_{i=1}^{N_b}\sum_{\alpha}\left\langle\left[(r_i)_\alpha - (r_{c.o.m})_\alpha\right]^2\right\rangle \tag{15}$$

where N_b is the number of beads within the polymer chain, the subscript *com* refers to the chain centre of mass and α represents x, y or z directions. The overlap between the two opposite layers can be quantified via the calculation of an interpenetration coefficient I defined as

$$I = \frac{\int_0^{\mathrm{L_z}/2}\mathrm{dz}\rho_1(\mathrm{z})}{\int_{-\mathrm{L_z}/2}^{\mathrm{L_z}/2}\mathrm{dz}\rho_1(\mathrm{z})}. \tag{16}$$

The height h of the brush layer is estimated from the first moment of the brushes as

$$h = \frac{\int_{-\mathrm{L_z}/2}^{\mathrm{L_z}/2}\mathrm{dz\,z}\rho_1(\mathrm{z})}{\int_{-\mathrm{L_z}/2}^{\mathrm{L_z}/2}\mathrm{dz}\rho_1(\mathrm{z})} \tag{17}$$

where $\rho_1(z)$ is the density profile of a single brush.

As the polymer brush system is sheared, the polymer chains tend to tilt in the direction of the imposed shear. The average orientation of the layer can be thus characterized by the director, **d**. It is the eigenvector corresponding to the largest eigenvalue of the **Q** tensor defined as $\mathbf{Q} = (1/N)(\sum_i \mathbf{e}_i\mathbf{e}_i - (1/3)I)$ where the sum is over all polymer chains. The internal ordering against the director can be estimated from the order parameter P_1 as

$$P_1 = \frac{1}{N}\left\langle \sum_i \mathbf{e}_i \cdot \mathbf{d}\right\rangle. \tag{18}$$

4. Thermodynamic stability of sheared polymer brushes in the constant-μVT ensemble

In the original DPD approach, the linear momentum, the number of particles and temperature are conserved. In this case the DPD model satisfies the condition of Galilean invariance [31] and detailed balance [32]. This makes DPD an attractive method to treat the problem of polymer-grafted surfaces under shear flow where hydrodynamics interactions may be significant. We have

also established that the use of the DPD model in the grand canonical ensemble is an efficient technique for determining the force-distance profiles of compressed equilibrium polymer brushes [23]. If we wish to study the rheological properties in the constant-μVT ensemble, we need to check the influence of the non-conservation of the total number of particles and momentum on the non-equilibrium properties such as the friction and shear viscosity.

To address this issue, we compare the thermodynamics, rheological and structural properties of the polymer brushes calculated from a simulation in the constant-μVT ensemble with those from a number of simulations in constant-NVT ensemble over the corresponding values of N. These comparisons are shown in table 1. Typically, for a system under moderate compression at h/h_0 of 0.6, the average number of solvent particles in the acquisition phase of the constant-μVT simulation is equal to 4905 ± 10, a variation of 0.2%. We have performed constant-NVT simulations across this range of N. In table 1, we show the thermodynamic properties (pressure components, chemical potential) and the rheological (friction and viscosity) properties as well as the structural parameters (layer width, orientational order, director). The results from the constant-NVT ensemble are unchanged within the estimated error when the total number of solvent particles varies by 10 units. Additionally, we show that the properties calculated at constant-μVT match those from the range of constant-NVT simulations. Once the equilibrium is reached in the grand ensemble, the variation of the number of solvent particles during the production phase does not affect the rheological properties of the system and we can confidently use of the DPD method in the grand canonical ensemble for a system under shear.

The equilibration phase in the grand canonical ensemble is an essential step to obtain the appropriate number of solvent particles for a given compression. We note that the variation of the number of solvent particles during equilibration between two consecutive surface separations can reach 800.

Figure 2(*a*) shows the configurational chemical potential profile $\mu^{\text{conf}}(z)$, calculated in the simulation of a sheared polymer brush system at constant chemical potential. As required the configurational chemical potential is constant for all z even if the solvent density profile is nonuniform. We also check that the calculated $\mu^{\text{conf}}(z)$ from the Widom insertion technique is equal to the externally fixed chemical potential. Figure 2(*b*) shows the configurational chemical potential calculated at constant-μVT and constant-NVT simulations at all compression ratios. The average value of $\mu^{\text{conf}}(z)$ deviates by less than 1% from the fixed chemical potential at all compressions, whereas at constant density the configurational chemical potential decreases dramatically with compression. Such constant-NVT simulations cannot be expected to model the experimental SFA where the solvent is in equilibrium with the reservoir at a fixed temperature and chemical potential. Although, we do not show these explicitly, the profiles of the local temperature and pressure components are also constant with z as required for thermal and mechanical equilibrium. These checks demonstrate both the efficiency and the stability of our methodology for polymer brushes under shear where the chemical potential of the external solvent is fixed.

The difference in the two approaches is illustrated in figure 3, which shows the total force between the surfaces as a function of the compression. This profile can be directly compared with experiment. In the figure, the experimental force-compression profile has been determined for poly(ethylene-propylene) chains grafted to mica surfaces in cyclohexane [9], the theoretical curve is obtained from the Alexander-de Gennes model [10, 12]. The experimental and theoretical curves are shifted vertically to match the simulated curves and we should only compare their shapes. In the simulation, these profiles are calculated by subtracting the normal pressure at the reference state, $h/h_0 = 1$ from the

Table 1. Thermodynamics ($-P_{xz}, P_{zz}, \mu_z^{\text{conf}}$), rheological ($\epsilon, \eta$) and structural ($Rg^2, I, h, d, P_1$) properties calculated in both constant-NVT simulations with different number of solvent particles (N) and constant-μVT simulations at h/h_0 of 0.6. All the properties are defined with their symbols in the parts of section 3.

N	$-P_{xz}$	P_{zz}	ϵ	η	μ_z^{conf}	Rg^2	I	h	d	P_1
Constant-μVT ensemble										
4905_{10}	5.35_1	116.2_3	0.0461_2	3.62_1	44.3_1	12.5_2	0.012_1	4.62_5	44.0_1	0.90_1
Constant-NVTensemble										
4905	5.46_2	115.8_3	0.0472_2	3.61_1	44.3_1	12.6_2	0.013_1	4.64_5	44.1_1	0.90_1
4895	5.47_2	115.6_3	0.0473_2	3.61_1	44.2_1	12.6_2	0.013_1	4.64_5	44.0_1	0.90_1
4915	5.47_1	116.0_3	0.0472_2	3.61_1	44.4_1	12.6_2	0.013_1	4.64_5	43.8_1	0.89_1

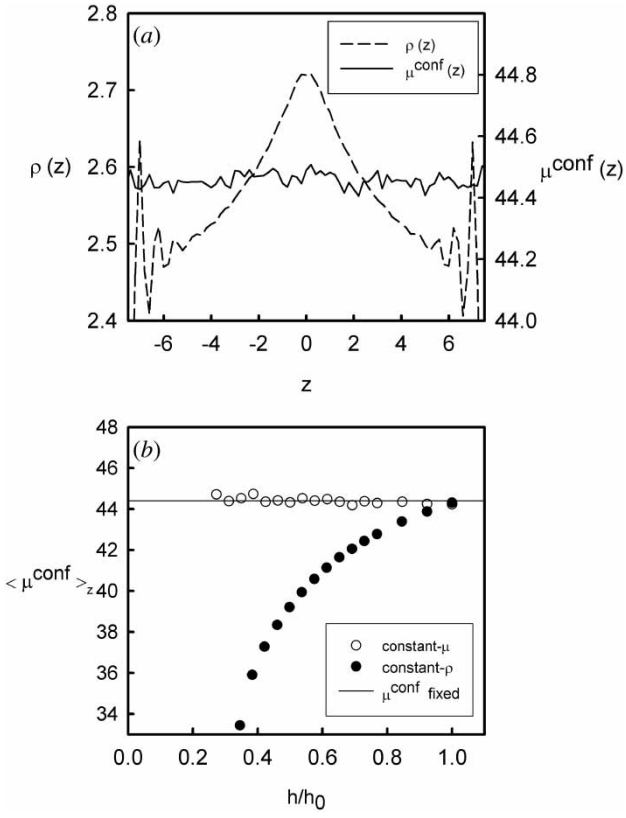

Figure 2. (*a*) The solvent density $\rho(z)$ (dashed line) and the configurational chemical potential $\mu^{\text{conf}}(z)$ (solid line) profiles from a constant-μVT simulations at $h/h_0 = 0.6$. (*b*) The calculated configurational chemical potential from the constant-NVT simulations at a constant density (black circles) and from the constant-μVT simulations (open circles) calculated from the Widom particle insertion method. The solid line shows the fixed value of chemical potential of the external resevoir.

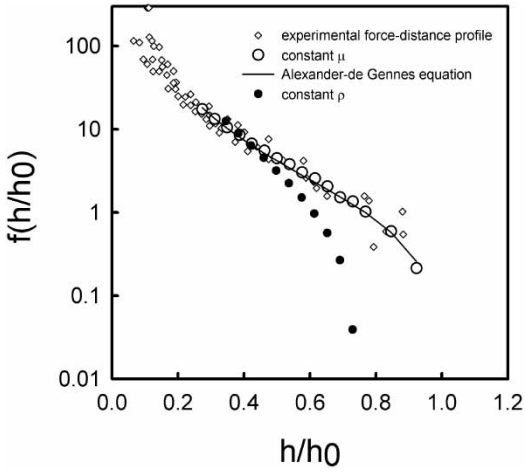

Figure 3. A semi-log plot of the experimental and simulated force-compression profiles. The solid line represents the profile calculated from the Alexander-de Gennes equation. The experimental and theoretical results have been shifted vertically to obtain the best agreement with the simulated data.

average normal pressure at h. The normal component is calculated from equations (10) and (11) and averaged over the z-dimension of the simulation box. We find excellent agreement between the simulations at constant-μVT and those from the SFA experiments [9]. Furthermore, the simulated profile is also in good agreement with that predicted by the Alexander-de Gennes theory. In contrast, the results obtained at constant density (i.e. from constant-NVT simulations with ρ fixed at all compressions) do agree well with the experiments particularly at high compression but are poorer at low compressions. This result has been already observed in the compression of equilibrium polymer brushes [23] but the discrepancies between the two models are more pronounced in the case of polymer brushes under shear.

Figure 4(*a*) displays the friction coefficient profile calculated from equation (13) averaged over the production phase of the simulation for two compressions. Firstly, we show that the friction coefficient is constant with z, allowing the calculation of a reliable average friction coefficient value. The inset shows the friction coefficient averaged over z as a function of time. The friction coefficient evolves around an equilibrium value with relative small deviations and the small fluctuation in the number of the solvent particle during the production phase affects neither the average value of ϵ or its evolution as a function of time.

5. Influence of the solvent, shear rate and surface coverage on the friction coefficient

This section contains the principal results of the paper. Figure 4(*b*) shows the friction coefficient as a function of compression for wet and dry brushes at two grafting densities and different shear rates. A dry brush consists of the grafted polymers without any solvent particle and consequently these simulations are performed in the constant-NVT ensemble. At fixed surface coverage and shear rate, we observe two quite different behaviours of the friction coefficient as a function of compression for the dry and wet brushes. The friction coefficient of dry brushes reduces exponentially as the system is compressed whereas it increases slightly with compression of the brushes in the presence of solvent. In all cases, the friction coefficient of the dry brushes is larger that that of the wet brushes indicating the lubricant properties of the solvent: the solvent particles assist the sliding of the brushes. As expected, the friction coefficients for the dry and wet brushes converge to the same value at the strongest compression, as the number of solvent particles in the layer is reduced.

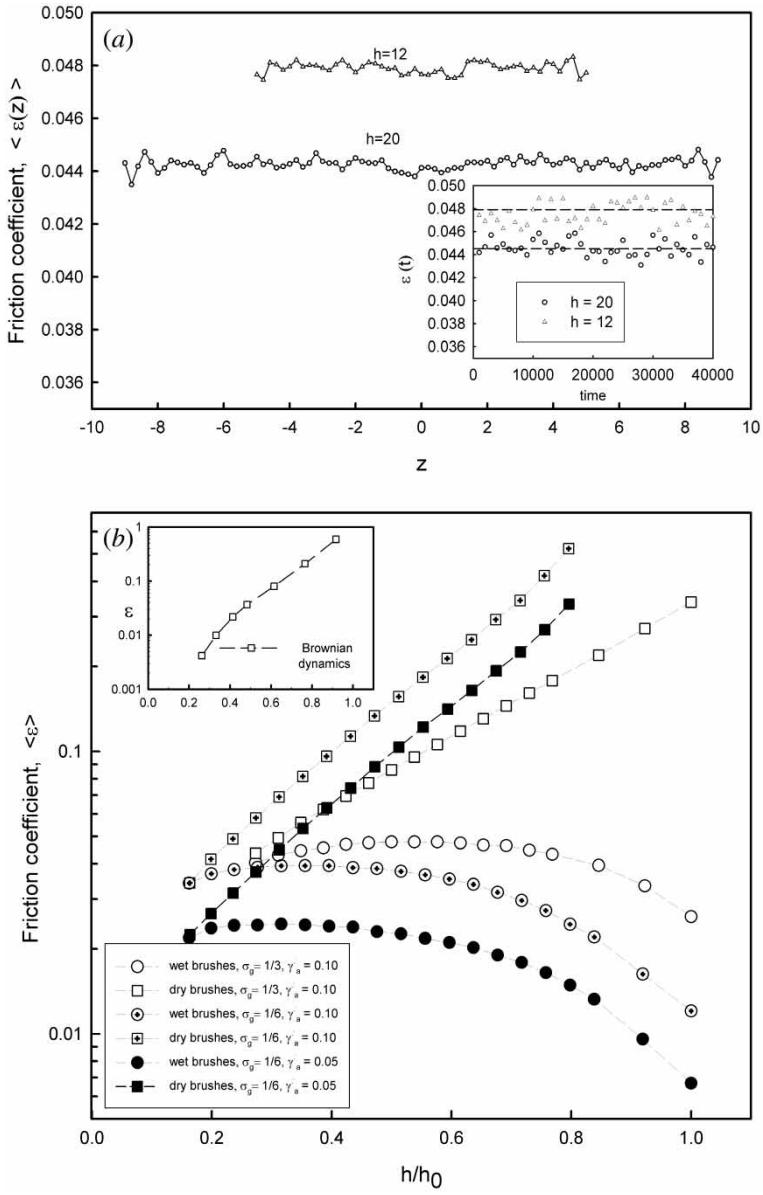

Figure 4. (*a*) The friction coefficient profiles for two separation distances accumulated over the total production phase of the simulation. The inset shows the variation of the mean friction coefficient at the same compressions. The friction $\epsilon(t)$ is averaged both across the pore and over short periods of time. (*b*) The mean friction coefficient as a function of the compression for dry and wet brushes at different shear rates and surface coverages. The inset shows the friction coefficient profile calculated in previous BD simulations [16].

The reduction in the friction of the dry brushes as the pore width is decreased is attributed to the fact that the grafted chains are only weakly entangled in the interfacial region [6] (the measured interpenetration coefficient is small) and that the tangential pressure increases more slowly than the normal pressure with a disordered fluid of polymer beads offering little resistance to shear. The main difference between this and the wet system occurs at $0.8 < h/h_0 < 1.0$ when the polymers layers are weakly interpenetrating. As shown in figure 2(*a*), the solvent particles are present both in the polymer region and in the interfacial region with a slightly higher density in the middle of the pore. Indeed the shear tends to reduce the height of the brush and forces more solvent particles into the central region. Under shear, the polymer chains escape the compression by tilting in the direction of the shear with an angle between the director of the layer and the normal to the surface close to 80° at the highest compressions. In these circumstances, the pure solvent

between layers acts a strong lubricator reducing the friction coefficient at this separation by one to two orders of magnitude. On further compression the solvent leaves the polymer brushes and the region between the plates and ϵ rises slightly to the same value as the dry brush.

There is some uncertainty in the SFA experiment on the precise surface coverage of the polymers. The simulations allow us to investigate this effect. For wet brushes lowering the surface coverage of the polymer reduces the friction and this more marked at weak compression. At the same external chemical potential more solvent must be introduced into the inter-layer region at lower coverage and the friction reduces. Interestingly, the opposite effect is seen with the dry brushes where increasing the surface coverage reduces the friction. In both cases, the shape of the friction-compression curve changes with coverage.

A reduced shear rate of 0.1 represents the top of the experimentally accessible range. If we decrease the shear rate by a factor of 2, the friction coefficient is reduced for both wet and dry brushes. The shape of the friction-compression curve is unchanged.

The friction coefficient calculated from the DPD simulations are in the range 0.05–0.1. These are slightly higher than values of 10^{-3} to 0.05 determined by Klein from SFA experiments [6]. We feel that the relative magnitudes of the normal and tangential forces is reasonably well reproduced by the DPD model. However, since the friction coefficient is the one absolute comparison that we can make with experiment, we would like to see more detailed work on ϵ as a function of compression, surface coverage and shear rate from the SFA. The friction-compression profile would be a particulary useful experimental measurement.

The inset to figure 4(*b*) shows the friction coefficient profile determined from Brownian dynamics simulations [16] of a polymer brush under steady and oscillatory shear. In this study, the solvent particles are not explicitly represented but treated as a continuum. The resulting friction profile is similar to that calculated from DPD simulations on dry brushes with approximately the same shape and absolute magnitude. The explicit presence of solvent particles dramatically changes this curve and should form a more reliable comparison with experiment as this becomes available.

6. Influence of the interaction conservative potential and of the solvent size

In this section, we consider two details of the DPD that might be expected to change the force and friction-compression curves and to estimate the size of these effects.

Firstly, we consider the influence of the steepness of the conservative potential between the segments of the polymer chain on the rheological properties. The random and dissipative forces are kept unchanged. These do not influence the interaction potential but could potentially influence the rheological properties. However, we feel that the form of the conservative potential is likely to make the most significant difference. From equation (3), the conservative force is written in terms of a weighting function $\omega_C(r_{ij})$. As DPD has been designed to model systems at a mesoscopic level, any weighting function $\omega_C(r_{ij})$ which we introduce should be repulsive and soft so that we can continue to model Kuhn segments of the polymer and still use a comparatively 'long' reduced time-step to allow for equilibration of these systems. Previous work on a truncated and shifted Lennard Jones potential in DPD [33] indicates that small timesteps are required and we were unable to obtain equilibration in our system with this type of model. Instead, we employed a simple extension of DPD model, where the conservative force is modelled as a linear ramp, by increasing the exponent of the weighting polynomial from 1 to 4 as follows

$$\begin{aligned}\omega_{C,1}(r_{ij}) &= (1 - r_{ij}/r_c)\\ \omega_{C,2}(r_{ij}) &= (1 - r_{ij}/r_c) + (1 - r_{ij}/r_c)^2\\ \omega_{C,3}(r_{ij}) &= (1 - r_{ij}/r_c) + (1 - r_{ij}/r_c)^2\\ &\quad + (1 - r_{ij}/r_c)^3 + (1 - r_{ij}/r_c)^4. \end{aligned} \tag{19}$$

These analytical expressions of the conservative forces are shown as an inset in figure 5. The other inset in figure 5 shows the pair correlation function $g(r)$ of a pure DPD fluid calculated using each weighting function $\rho = 5.0$ and $T = 2.0$. As expected, the addition of the higher order polynomial contributions in the conservative interaction increases both the excluded volume between particles and the magnitude of the first peak in $g(r)$. We have performed the compression of polymer brushes at constant chemical potential using both the $\omega_{C,2}(r_{ij})$ and $\omega_{C,3}(r_{ij})$ weighting functions. As the thermodynamics of a DPD system is governed by the conservative force, we need to calculate the configurational chemical potential values of the solvent in the reference system for $\omega_{C,2}(r_{ij})$ and $\omega_{C,3}(r_{ij})$ weighting functions. They are equal to 55.6 and 59.4 for $\omega_{C,2}(r_{ij})$ and $\omega_{C,3}(r_{ij})$, respectively. For $\omega_{C,1}(r_{ij})$, the chemical potential was maintained at 44.4. We check that changing the potential does not affect the thermodynamical, mechanical and chemical equilibria of our systems. The structural properties of the polymer brushes are unchanged along the compression curve

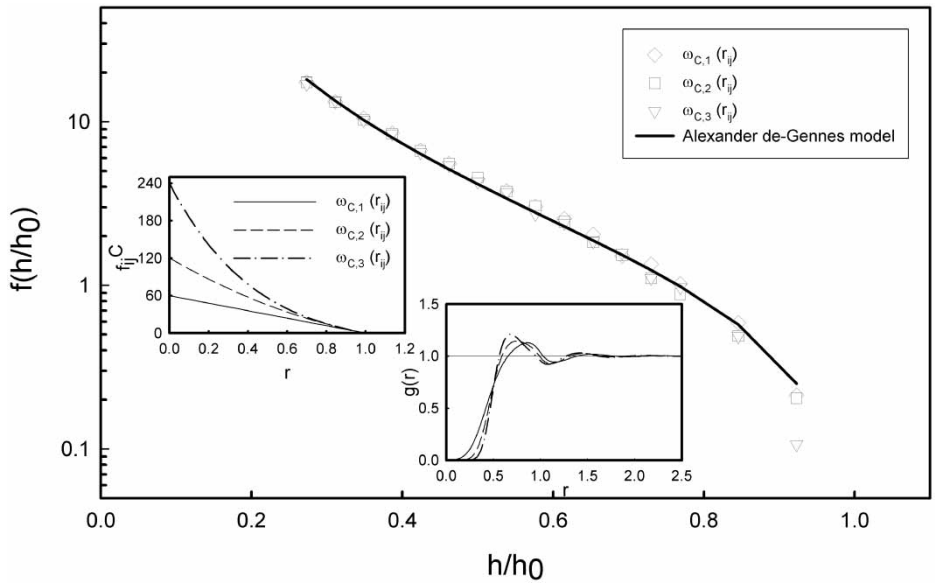

Figure 5. The normal force-compression profiles calculated in polymer brushes using the different forms of the conservative potential. The leftmost inset shows the shape of the conservative force and the rightmost the corresponding pair correlation function $g(r)$ for a pure DPD fluid with the different conservative potentials.

when the potential becomes more repulsive. Obviously, the magnitude of the pressure components increases with the repulsiveness of the potential. However, figure 5 shows that the normalized force-compression profile does not depend on the precise analytical forms we have used for the conservative potential over the range that we have employed. In addition, the friction-compression profiles, figure 6(*a*), show that the friction can be considered to be independent of the shape of the conservative potential in this range. It is not possible to extract a correlation between the friction and the repulsiveness of the potential. In all cases, the variations observed when we change the potential are very small compared to those caused by the change of the shear rate or the surface coverage. We conclude that changes in the form of the conservative potential in this range do not affect the structural properties, the force-distance and friction profiles.

In the DPD model the solvent is represented as a soft particle often of the same size as the polymer bead. In this study, we will explore how the size of the solvent particle might affect the friction coefficient by changing the cutoff radius of the solvent-solvent interactions from 1.0 to 0.5. The cutoff radius for the solvent-polymer interactions is

$$r_c^{\mathrm{pol-sol}} = 0.5\left(r_c^{\mathrm{pol-pol}} + r_c^{\mathrm{sol-sol}}\right) \tag{20}$$

while the cutoff value is kept at 1.0 for the polymer–polymer interactions. When the cutoff radius was set to 1.0 for all the interactions, the number of solvent

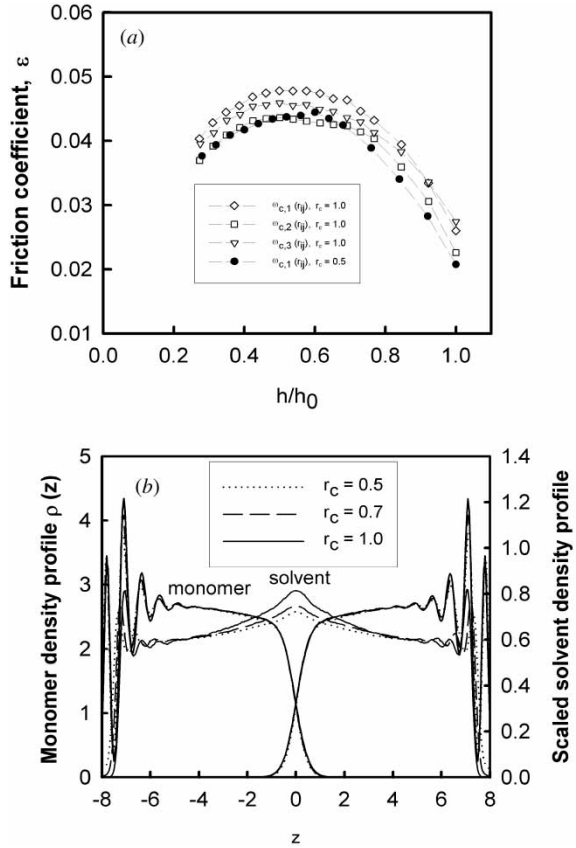

Figure 6. (*a*) The friction coefficient profiles calculated for each of the three conservative potential forms and for a smaller size of solvent particle ($r_c = 0.5$). (*b*) The monomer and solvent density profiles calculated for three sizes of solvent particles.

particles in the reference system ($h = h_0$) was around 8300. Decreasing the cutoff for the solvent–solvent interactions to 0.5 means increasing number of solvent particle close to 40000 to keep the packing fraction of the solvent approximately constant. This increases the simulation time by a factor of ca. 10. Figure 6(*b*) shows the polymer density profiles as function of the cutoff radius. We observe that they are unchanged when the size of the solvent is decreased. An analysis of the amount of interpenetration, the brush thickness and orientational ordering confirms that the structural properties of the polymer brushes do not depend on the size of the solvent particle. Figure 6(*b*) also shows the profiles of the solvent particles for three sizes of solvent. Theses profiles are scaled by $(r_c^{\mathrm{sol-sol}})^3$ to effect a sensible comparison. The scaled profiles of the solvent density become slightly flatter in the middle of the pore when the size is smaller whereas they are identical in the polymer regions. We would expect the solvent density profile to become more uniform as the solvent becomes more discrete. In figure 6(*a*), the black circles show that the reduction of the solvent particle decreases the friction coefficient slightly but does not change the shape of the friction profile. Again these effects are small compared to changes in shear rate and surface coverage.

7. Conclusions

We have performed mesoscopic simulations to study the rheological properties of grafted polymer brushes under shear and compression. We have shown that the methodology of keeping the chemical potential of the solvent constant during the compression curve provides reliable force-compresion profiles in comparison with experiment compared to a model where the total density is constant. We demonstrate that the addition or removal of solvent particles does not affect the thermodynamic and rheological properties of the polymer brushes system once the equilibrium is reached. We also show that the implementation of shear in the methodology at constant chemical potential conserves the thermodynamic equilibria and thus represents an appropriate technique for the study of compressed polymer brushes under shear.

We have addressed a certain number of fundamental questions concerning both the variation of the friction and the normal forces along the compression curve and the influence of the shear rate, grafting density, conservative potential form and size of the solvent on the friction coefficient profiles.

We have shown that explicit inclusion of the solvent particles dramatically changes the friction-compression profiles and confirmed the lubricant properties of the solvent in the wet brushes. This effect is more marked than the change in the force-compression profile. We have established that the variations of the friction coefficient as a function of the separation kept the same shape when the surface coverage and shear rate have been reduced. The magnitude of the friction coefficient depends on both the surface coverage and the shear rate. The normal force-distance and friction profiles have been shown to be independent on the form of the conservative potential so long as the conservative potential is kept repulsive and soft. We do not detect any major influence of the size of the solvent particle on the structural properties of the brushes or on the friction coefficient profile. The change in the magnitude of the friction caused by the reduction of the solvent particle size is small compared to those induced by the changes in the shear rate or grafting density.

Acknowledgements

F. G. and P. M. are grateful to Unilever Research for its financial support in completing these simulations.

References

[1] J. Klein. *Annu. Rev. Mater. Sci.*, **26**, 581 (1996).
[2] J. Klein, D. Perahia, S. Warburg. *Nature*, **352**, 143 (1991).
[3] H.J. Taunton, C. Toprackcioglu, J. Klein. *Macromolecules*, **21**, 3336 (1988).
[4] H.J. Taunton, C. Toprackcioglu, L.J. Fetters, J. Klein. *Macromolecules*, **23**, 571 (1990).
[5] J. Klein, Y. Kamiyama, H. Yoshizawa, J.N. Israelachvili, G.H. Fredrickson, P. Pincus, L.J. Fetters. *Macromolecules*, **26**, 5552 (1993).
[6] J. Klein. *Colloids Surfaces A: Physicochem. Eng. Aspects*, **86**, 63 (1994).
[7] J. Klein, E. Kumacheva, D. Mahalu, D. Perahia, L.J. Fetters. *Nature*, **370**, 634 (1994).
[8] J. Klein, E. Kumacheva, D. Mahalu, D. Perahia, L.J. Fetters. *Acta Polym.*, **49**, 617 (1998).
[9] R. Tadmor, J. Janik, J. Klein, Fetters, L.J, *Phys. Rev. Lett.*, **91**, 115503-1 (2003).
[10] S. Alexander. *J. phys.* (Paris), **38**, 983 (1977).
[11] P.G. de Gennes. *Macromolecules*, **13**, 1069 (1980).
[12] P.G. de Gennes. *ph Adv. Colloid Interface Sci.*, **27**, 189 (1987).
[13] S.T. Milner, T.A. Witten, M.E. Cates. *Macromolecules*, **21**, 2610 (1988).
[14] S.T. Milner. *Science*, **251**, 905 (1991).
[15] G.S. Grest. *Curr. Opin. Colloid Interface Sci.*, **2**, 271 (1997).
[16] S.P. Doyle, Shaqfeh, E.S.G., A.P. Gast. *Macromolecules*, **31**, 5474 (1998).
[17] T. Kreer, M.H. Müser, K. Binder, J. Klein. *Langmuir*, **17**, 7804 (2001).
[18] T. Kreer, Müser, M.H., K. Binder. *Comput. Phys. Commun.*, **147**, 358 (2002).

[19] T.A. Vilgis, A. Johner, J.F. Joanny. *Phys. Chem. Chem. Phys*., **1**, 2077.
[20] T. Kreer, M.H., Müser. *Wear*, **254**, 827 (2003).
[21] P. Malfreyt, D.J. Tildesley. *Langmuir*, **16**, 4732 (2000).
[22] D. Irfachsyad, D.J. Tildesley, P. Malfreyt. *Phys. Chem. Chem. Phys*., **4**, 3008 (2002).
[23] F. Goujon, P. Malfreyt, D.J. Tildesley. *Chem. Phys. Chem*., **5**, 457 (2004).
[24] P. Espanol, P.B. Warren. *Europhys Lett*., **30**, 191 (1995).
[25] R.D. Groot, P.B. Warren. *J. chem. Phys*., **107**, 4423 (1997).
[26] J.P.R.B. Walton, D.J. Tildesley, J.S. Rowlinson. *Molec. Phys*., **48**, 1357 (1983).
[27] J.P.R.B. Walton, D.J. Tildesley, J.S. Rowlinson. *Molec. Phys*., **58**, 1013 (1986).
[28] B. Widom. *J. stat. Phys*., **19**, 563 (1978).
[29] J.G. Powles, S.E. Baker, W.A.B. Evans. *J. chem. Phys*., **101**, 4098 (1994).
[30] J.G. Powles, B. Holtz, W.A.B. Evans. *J. chem. Phys*., **101**, 7804 (1994).
[31] P.J. Hoogerbrugge, J.M.V.A. Koelman, *Europhys. Lett*., **21**, 363 (1993).
[32] P.V. Coveney, P. Espanol. *J. phys.* A, **30**, 779 (1997).
[33] I. Vattulainen, M. Karttunen, G. Besold, J.M. Poison. *J. chem. Phys*., **116**, 3967 (2002).